Removing a Hydrogen Bond in the Dimer Interface of *Escherichia coli* Manganese Superoxide Dismutase Alters Structure and Reactivity[†,‡]

Ross A. Edwards,[§] Mei M. Whittaker,[||] James W. Whittaker,*[,||] Edward N. Baker,*[,⊥] and Geoffrey B. Jameson*[,§]

Centre for Structural Biology, Institute of Fundamental Sciences, Massey University, Palmerston North, New Zealand, Department of Biochemistry and Molecular Biology, Oregon Graduate Institute of Science and Technology, 20000 NW Walker Road, Beaverton, Oregon 97006-8921, and School of Biological Sciences and Department of Chemistry, University of Auckland, Auckland, New Zealand

Received October 16, 2000; Revised Manuscript Received January 24, 2001

ABSTRACT: Among manganese superoxide dismutases, residues His30 and Tyr174 are highly conserved, forming part of the substrate access funnel in the active site. These two residues are structurally linked by a strong hydrogen bond between His30 NE2 from one subunit and Tyr174 OH from the other subunit of the dimer, forming an important element that bridges the dimer interface. Mutation of either His30 or Tyr174 in *Escherichia coli* MnSOD reduces the superoxide dismutase activity to 30−40% of that of the wt enzyme, which is surprising, since Y174 is quite remote from the active site metal center. The 2.2 Å resolution X-ray structure of H30A-MnSOD shows that removing the Tyr174→His30 hydrogen bond from the acceptor side results in a significant displacement of the main-chain segment containing the Y174 residue, with local rearrangement of the protein. The 1.35 Å resolution structure of Y174F-MnSOD shows that disruption of the same hydrogen bond from the donor side has much greater consequences, with reorientation of F174 having a domino effect on the neighboring residues, resulting in a major rearrangement of the dimer interface and flipping of the His30 ring. Spectroscopic studies on H30A, H30N, and Y174F mutants show that (like the previously characterized Y34F mutant of *E. coli* MnSOD) all lack the high pH transition of the wt enzyme. This observation supports assignment of the pH sensitivity of MnSOD to coordination of hydroxide ion at high pH rather than to ionization of the phenolic group of Y34. Thus, mutations near the active site, as in the Y34F mutant, as well as at remote positions, as in Y174F, similarly affect the metal reactivity and alter the effective pK_a for hydroxide ion binding. These results imply that hydrogen bonding of the H30 imidazole N−H group plays a key role in substrate binding and catalysis.

Superoxide dismutases (SODs)[1] are ubiquitous antioxidant metalloenzymes that catalyze disproportionation of superoxide through a two-step, one-electron redox cycle (*1*−*3*)

$$O_2^{-\bullet} + M^{n+} \rightarrow O_2 + M^{(n-1)+} \quad (1a)$$

$$O_2^{-\bullet} + 2H^+ + M^{(n-1)+} \rightarrow H_2O_2 + M^{n+} \quad (1b)$$

yielding an overall reaction

$$2O_2^{-\bullet} + 2H^+ \rightarrow O_2 + H_2O_2 \quad (2)$$

All SODs are able to catalyze the disproportionation of superoxide at rates close to the diffusion limit (*4*, *5*). Four kinds of redox-active metal cofactors have been found in superoxide dismutases, with M = Cu−Zn, Fe, Mn, and Ni in different members of this family (*6*−*9*). Fe- and MnSODs share extensive structural and sequence homology and a mechanism in which the metal ion oxidation state alternates between II and III (*10*−*12*). The metal-binding site of all Fe- and MnSODs is absolutely conserved in structure and sequence, and the outer coordination sphere and secondary structure elements involved in forming the site are also highly conserved. All Fe- and MnSODs are based on a dimer organization within which the dimer interface is highly conserved. Many Fe and MnSODs further associate into tetramers. A growing number of medium- to high-resolution structures of wild-type and mutant Fe- and MnSODs (*13*−*37*) have been reported, providing clues to the roles played by selected residues in the second coordination shell surrounding the metal center. Substrate access to the active site occurs via a solvent-filled funnel that leads from the outside surface of the protein toward the metal-binding site of each monomer, terminating at the metal-bound solvent molecule

[†] This work is supported by grants from the Marsden Fund of New Zealand (MAU606 to G.B.J. and E.N.B.), the Lottery Health Grants Board of New Zealand (to G.B.J. and E.N.B.), and the National Institutes of Health (GM42680 to J.W.W.).

[‡] Atomic coordinates have been deposited with the Protein Data Bank, accession codes 1io8 (H30A mutant) and 1ioh (Y174F mutant).

* To whom correspondence should be addressed. G.B.J.: telephone (+64) 6 350 5799; Fax (+64) 6 350 5682; e-mail G.B.Jameson@massey.ac.nz. E.N.B.: telephone (+64) 9 373 7599; Fax (+64) 9 373 7619; e-mail Ted.Baker@auckland.ac.nz. J.W.W.: telephone 503 748 1065; Fax 503 690 1464; e-mail jim@bmb.ogi.edu.

[§] Massey University.

[||] Oregon Graduate Institute of Science and Technology.

[⊥] University of Auckland.

[1] Abbreviations: RMS, root mean square; SOD, superoxide dismutase; UV, ultraviolet; wt, wild type.

10.1021/bi002403h CCC: $20.00
Published on Web 03/20/2001

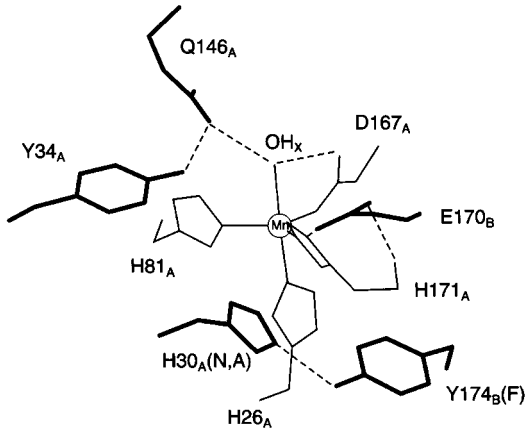

FIGURE 1: Active-site structure of *E. coli* MnSOD. Outer-sphere and gateway residues are highlighted in bold.

(*13*). For each metal center the funnel is comprised of residues contributed by both subunits. Four highly conserved residues at the bottom of the funnel in *Escherichia coli* MnSOD (Tyr34, His30, Trp169, and Glu170) partly shield the active site from the bulk solvent. A small hole between the closely packed side chains allows small anions and solvent to enter the active site. Because substrate access to the active site must involve these groups, they have been termed "gateway" residues (*38*). Of the second-shell residues, Tyr34 and Glu170, which arise from opposite subunits, are absolutely conserved, and His30 and Trp169 are conservatively substituted by asparagine and phenylalanine, respectively, in only a few of the more than 80 Fe- and MnSODs that have been sequenced to date. As illustrated in Figure 1, Tyr34 in wt enzymes has indirect contact with the metal through a putative hydrogen-bonding relay linking Tyr34 OH to Gln146 NE2 (or His146 NE2) and Gln146 NE2 (or His146 CE1) to the coordinated solvent species, OH^-/H_2O. The role of this relay in enzymatic function was the subject of a recent paper (*37*) describing the Y34F, Q146H, and Q146L mutants of the MnSOD from *E. coli* and has been the subject of several publications for human mitochondrial MnSOD (*32*−*35*).

Two highly conserved structural features involving the dimer interface and residues in the second coordination shell have been found in all Fe- and MnSOD structures solved to date. The first involves the carboxylate side chain of Glu170 and one of the metal ligands, His171. The glutamate side chain links subunits within the dimer, forming an outer-sphere salt bridge with the metal center in the other subunit, which bears a net +1 charge in both oxidation states. Mutation of Glu170 to alanine destabilizes the dimer interface, resulting in dissociation of the protein into monomers (*39*). A second feature involves a strong hydrogen bond between atom NE2 of the gateway histidine (His30) and atom OH of tyrosine (Tyr174) from the other subunit. This hydrogen bond has been found in all structures of wt enzyme determined so far. Tyr174 is absolutely conserved across all Fe- and MnSODs, although the sequence data available for 14 MnSOD species did not extend as far as this residue (*40*). The hydrogen bond to Tyr174 OH is very likely also conserved for all Mn- and FeSODs, including the FeSOD from *Pseudomonas aeruginosa* (*41*) and the MnSOD from maize (*42*), for which asparagine conservatively substitutes for the otherwise ubiquitous histidine at position 30 (*E. coli* numbering). The position and orientation of His30 are expected, therefore, to be strongly constrained by this highly conserved hydrogen-bonding interaction. This constraint may be important for function, allowing His30 to serve as a proton delivery site in the catalytic mechanism or to specifically interact with the substrate as it enters the active site.

In the work described here, the H30A, H30N, and Y174F mutants of *E. coli* MnSOD have been prepared and their structures have been solved, allowing us to investigate the roles of His30 and Y174 in the enzymatic mechanism. Structure−function correlations for these and other mutants of Fe- and MnSODs are used to develop structural insights into the mechanisms that permit substrates and products to enter and leave the narrow active site funnel at close to diffusion-controlled rates. The Y174F mutant is of special interest, in that it exhibits the greatest difference yet found between wt and mutant structures for the entire set of structurally characterized native and mutant Fe- and MnSODs. This result is significant in that the structure may represent a "snapshot" showing one extreme of the subunit arrangements achieved through the conformational flexibility of wt molecules in solution.

MATERIALS AND METHODS

Biochemical Preparation and Spectroscopic Characterization. The pDT1-5 antibiotic-resistant plasmid containing the *sodA* locus (*43*) was a generous gift of Dr. Danièle Touati (Institut Jacques Monod, Centre National de la Récherche Scientifique, Université Paris VII). This plasmid was used as a template for the production of all mutant plasmids using the Stratagene QuickChange in vitro site-directed mutagenesis procedure as previously described (*39*). Sequences of the mutant plasmids were verified by DNA sequence analysis (Molecular Biology Core Facility, Oregon Primate Research Center, Beaverton, OR) of the entire structural gene. The mutant plasmids were transformed into *E. coli* QC781 (*44*) sod A^- cells for protein expression. *E. coli* was grown as described previously (*39*), except the medium was supplemented with either 1 mM Mn(II) salts or 1 mM Fe(II) salts. Superoxide dismutase was purified as previously described (*45*). SOD activity was measured using the xanthine oxidase/cytochrome *c* inhibition assay (*6*). Protein concentration was determined by optical absorption measurements using the previously reported molar extinction coefficient ($A_{280} = 8.66 \times 10^4\ M^{-1}\ cm^{-1}$) (*46*). Metal quantitation was performed by atomic absorption spectrometric analysis using a Varian SpectrAA 20B atomic absorption spectrometer equipped with a GTA-96 graphite furnace.

Optical absorption spectra of the proteins were recorded on a Varian Cary5 UV−vis−NIR absorption spectrometer. The H30A mutant protein was converted to the oxidized Mn(III) form before optical spectrometry by treating the sample with excess molybdicyanide (*45*) followed with desalting by gel filtration.

Crystallization. Crystals of H30A-MnSOD were grown in sitting drops at room temperature by the method of vapor diffusion. The well solution contained 16−20% PEG 6000 and 0.1 M bicine titrated between pH 8.0 and pH 8.3, with initial protein concentrations of 18−20 mg mL^{-1} in the sitting

Table 1: Data Collection and Reduction Statistics for *E. coli* H30A- and Y174F-MnSOD

crystal	H30A-MnSOD	Y174F-MnSOD
space group	$C222_1$	$P2_1$
Z (Z')	32 (4)	4 (2)
unit cell	$a = 100.681$ Å	$a = 46.893$ Å
	$b = 109.110$ Å	$b = 46.017$ Å
	$c = 181.072$ Å	$c = 95.993$ Å
		$\beta = 98.4°$
V(m)	2.76 Å^3/Da	2.28 Å^3/Da
solvent content	55%	46%
mosaicity	0.25°	0.21°
data collection temp	293 K	110 K
data collection device	RU200B/RAxisIIC	Mar345/DESY/X11
wavelength/monochromation	1.54 Å/graphite crystal	0.91 Å/bent Ge crystal
data processing		
resolution limits (of last shell)	40−2.2 Å (2.25−2.20)	50−1.35 Å (1.37−1.35)
unique reflections	50905	89143
obsd reflections	458707	561459
obsd reflections after averaging	255035	373356
obsd reflections after merging	48514	89109
observations deleted manually	666	142
redundancy	5.3	4.2
completeness	95.3% (73.0)	100.0% (99.9)
R_{merge}[a] on intensities	0.059 (0.259)	0.027 (0.071)
overall I/σ	22.4 (4.0)	52.5 (18.3)

[a] $R_{merge} = \sum|I - \langle I\rangle|/\sum I$, where $\langle I\rangle$ is the mean of individual observations of intensities I.

drop, which typically comprised 2 μL of protein solution in 0.1 M bicine plus 2 μL of well solution. Crystals formed as hexagonal blocks rather than the elongated blocks of the wild-type enzyme. Only with polypropylene wells (instead of the more commonly used polyethylene wells) was suitably crystalline material obtained. Crystals of Y174F were grown under similar conditions and formed large elongated blocks, the largest having dimensions of approximately 0.5 × 0.5 × 2−3 mm.

X-ray Diffraction, Data Collection, and Structure Refinement. Although isomorphous with wt MnSOD, many crystals of H30A-MnSOD were tried before one suitable for data collection could be found, as crystals of this mutant are very much more fragile than those of wt, or of mutants Q146H, Q146L, and Y34F. The images were subsequently indexed and integrated to 2.2 Å using the program DENZO (*47*). The program SCALEPACK (*47*) was used to scale and merge the resulting data. The reflections flagged for calculation of R_{free} corresponded to those selected for R_{free} in the wt data set (*18*). Relevant data collection and processing statistics are given in Table 1. The structure of the H30A mutant was solved using molecular replacement [AMORE (*48*)] with the AB dimer of Q146L as the search model for two copies of the dimer in the asymmetric unit. Solvent waters, the metal ion, and the solvent-bound hydroxide were not included in the search model, and Leu146 was changed to Gln and His30 to Ala. Model building was carried out using the graphics program TURBO FRODO (*50*). Refinement of atomic coordinates and temperature factors against maximum-likelihood target functions (*51*) was carried out using CNS (development version 0.5) (*49*). Refinement and model statistics are given in Table 2.

Data for Y174F-MnSOD were indexed and integrated to 1.35 Å using the program DENZO (*47*). The program SCALEPACK (*47*) was used to scale and merge the resulting data. A resolution of 1.35 Å, rather than the limit of 0.90 Å to which data were collected, was deemed sufficient for analysis and comparison with wt and the other *E. coli* mutants, H30A, Y34F, Q146H, and Q146L. Complete analysis of Y174F using the data collected to 0.90 Å will be presented in detail elsewhere. The relevant data collection and processing statistics are presented in Table 1. The structure of Y174F was solved similarly to H30A, except that the asymmetric unit contained only a single dimer. The model of Y174F-MnSOD was originally refined against data collected to 1.5 Å on the in-house facility. The partly refined model, missing Mn atoms and solvent water molecules, was used as the starting model for refinement against the 1.35 Å data. SHELXL (Release 97-2) (*52*) was used to refine the structure. Final refinement and model statistics are given in Table 2. No noncrystallographic symmetry restraints on either positional parameters or temperature factors were applied to the 1.35 Å refinement in SHELXL. The average main-chain temperature factor for subunit A is 8.3 Å^2, and the average main-chain temperature factor for subunit B is 10.8 Å^2.

Table 2: Refinement and Model Statistics for *E. coli* H30A- and Y174F-MnSOD

model	H30A	Y174F
no. of residues	820	410
no. of protein atoms	6492	3254
no. of water molecules	255	498
no. of Mn ions	4	2
average temp factors (Å^2)		
main-chain atoms	23.9	9.5
side-chain atoms	25.3	25.1
water molecules	28.3	18.1
manganese ions	14.5	6.1
overall	24.7	11.2
refinement		
refinement program	CNS v0.5	SHELXL
reflections used in refinement	48504	84648
reflections used in R_{free} calcn	2456 (5.1%)	4444 (5.2%)
resolution limits	40.0−2.2 Å	50.0−1.35 Å
RMS bond lengths	0.005 Å	0.005 Å
RMS bond angles	1.16°	1.34°
Ramachandran plot		
most favored regions	91.1%	92.0%
additional allowed regions	7.5%	6.6%
generously allowed regions	0.8%	1.4%
disallowed regions	0.6%	0.0%
R[a] (all data)	0.184	0.170
R_{free} (all data)	0.211	0.196

[a] $R = \sum(|F_o| - |F_c|)/\sum|F_o|$, where $|F_o|$ and $|F_c|$ are the observed and calculated structure factor amplitudes, respectively.

Table 3: Catalytic Activity for *E. coli* Mutants

MnSOD mutant	SOD activity (units/mg) Mn	Fe
wt	7300	60
H30A	2200	190
H30N	2800	10
Y174F	3000	110

RESULTS

Superoxide Dismutase Activity. Mn forms of the H30A, H30N, and Y174F mutants all show a significant decrease in catalytic activity (Table 3) compared to wt MnSOD (*45*). Mutation of either His30 or its hydrogen-bonding partner

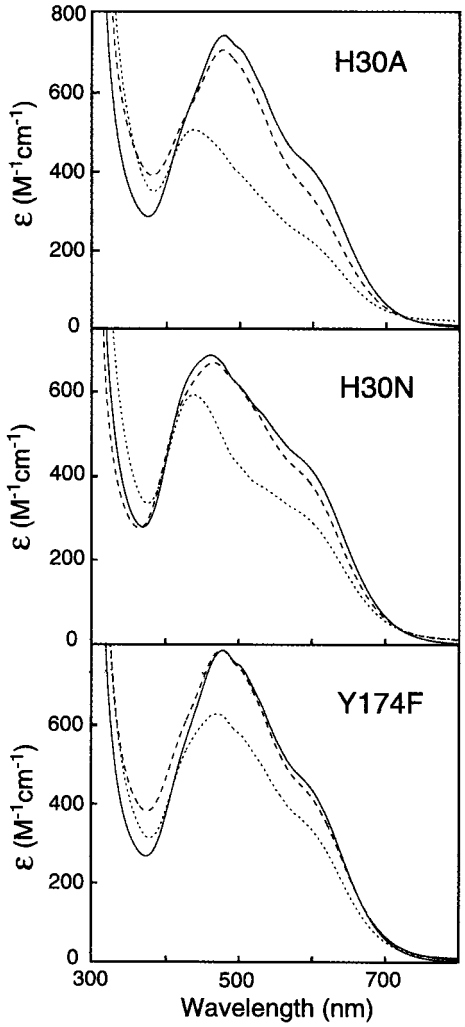

FIGURE 2: Optical absorption spectra for Mn(III) SOD mutants. (Upper) H30A-MnSOD following treatment with molybdicyanide: (solid line) in 50 mM potassium phosphate buffer, pH 7; (dashed line) in 50 mM CAPS buffer, pH 10.5; (dotted line) in the presence of 100 mM sodium azide at pH 7 (K_d = 6 mM). (Middle) H30N-MnSOD as isolated: (solid line) in 50 mM potassium phosphate buffer, pH 7; (dashed line) in 50 mM sodium pyrophosphate buffer, pH 9.2; (dotted line) in the presence of 100 mM sodium azide at pH 7 (K_d = 10 mM). (Lower) Y174F-MnSOD as isolated: (solid line) in 50 mM potassium phosphate buffer, pH 7; (dashed line) in 50 mM CAPS buffer, pH 10.5; (dotted line) in the presence of 100 mM sodium azide at pH 7 (K_d = 11 mM).

Tyr174 gives a similar reduction of SOD activity (30−40% of wt MnSOD). For each of these mutants, the Fe-substituted forms have considerably lower activity than their Mn-containing counterparts, as previously found for the Fe-substituted wt MnSOD. The Fe-substituted form of H30N MnSOD is noticeably less active than the other mutants.

Optical Absorption Spectra of MnSOD Mutants. The optical absorption spectra of the Mn(III) forms of H30A- and Y174F-MnSOD closely resemble the spectrum of wt Mn(III)SOD having a maximum absorption peak near 480 nm with extinction coefficients in the range 700−800 M^{-1} cm^{-1}, slightly lower than the 850 M^{-1} cm^{-1} of the wt enzyme (*45*). However, the spectrum of Y174F MnSOD is slightly sharper around the absorption maximum (Figure 2). The optical absorption spectrum of Mn-containing H30N-MnSOD shows features typical of a five-coordinate Mn(III) metal center; however, the maximum absorption peak is shifted to higher energy (∼15 nm) compared to the wt Mn(III)SOD (*45*), and the H30N mutant has a distinct pattern of fine structure arising from spin-forbidden electronic transitions (Figure 2). Increasing pH has very little effect on the optical absorption spectra for all three mutants (Figure 2), although addition of azide shifts the absorption maximum and lowers intensity as observed for wt MnSOD (*38*, *45*).

General Comments on Structural Results. Mutation of Tyr174 to phenylalanine or mutation of His30 to alanine removes the 2.60 (3) Å[2] hydrogen bond between Tyr174 OH of one subunit and His30 NE2 of the other subunit. Because of 2-fold NCS symmetry, there is a pair of such hydrogen bonds spanning the dimer interface. This pair of hydrogen bonds provides two of the seven hydrogen bonds that span the dimer interface. In addition, His30 lies at the base of the substrate access funnel that leads to the metal active site. Disruptions to the dimer interface, changes in conformers of side chains, and changes in orientation of subunits comprising the dimer are far more extensive for the Y174F mutation than for the H30A mutant, which, except for the site of mutation, is closely superimposable on wt MnSOD (*18*) [and on Q146H, Q146L, and Y34F mutants (*37*)]. Figure 3a shows the overlay of the dimers of wt, H30A-MnSOD, and Y174F-MnSOD, based upon the superposition calculated for a single subunit (top molecule in Figure 3a). Pairwise superpositions of mutant and wt MnSOD are shown in the vicinity of the site of mutation in Figure 3b (His30A) and Figure 3c (Y174F).

The RMS differences for the pairwise superposition of subunuits of H30A (all 205 residues) and Y174F mutants (omitting residues 204 and 205) onto subunits of wt MnSOD range from 0.2 to 0.3 Å. This range is comparable to that of 0.14 to 0.35 Å observed for pairwise superpositions of the four subunits of wt MnSOD. However, as is apparent in Figure 3a, individual subunits of Y174F superimpose less well onto individual subunits of wt MnSOD (and also onto each other) than do the subunits of the H30A mutant. The similarity in RMS differences is an artifact arising from large differences in conformation of residues 134−136 among the four subunits of wt; these residues are involved in interdimer contacts not present in the Y174F structure.

As is apparent in Figure 3a, dimers of H30A-MnSOD superimpose closely on dimers of wt MnSOD with RMS differences in the range of 0.2 to 0.3 Å, similar to the value of 0.25 Å for the superposition of the AB dimer onto the CD dimer of wt MnSOD (*18*). On the other hand, the different quaternary structure of the Y174F mutant (see Figure 3, panels a and c) leads to RMS differences of 0.98 and 0.85 Å for the superposition of the dimer of Y74F onto the AB and CD dimers of wt MnSOD (again omitting residues 204 and 205 from the superpositions).

The H30A mutant is isomorphous with the crystal structure of not only the wt but also the Q146L, Q146H, and Y34F mutants of MnSOD of *E. coli*. The Y174F mutant is,

[2] Here and elsewhere the scatter of values about their mean is presented in parentheses, where the digit in parentheses corresponds to the uncertainty in the least significant digit of the parameter. For example, 2.60 (3) Å stands for 2.60 ± 0.03 Å. For wt, H30A-, Q146H-, Q146L-, and Y34F-MnSOD, the scatter is the estimated standard deviation calculated over the four NCS-restrained molecules. For Y174F-MnSOD, the scatter is the average deviation from the mean, as there are only two molecules in the asymmetric unit.

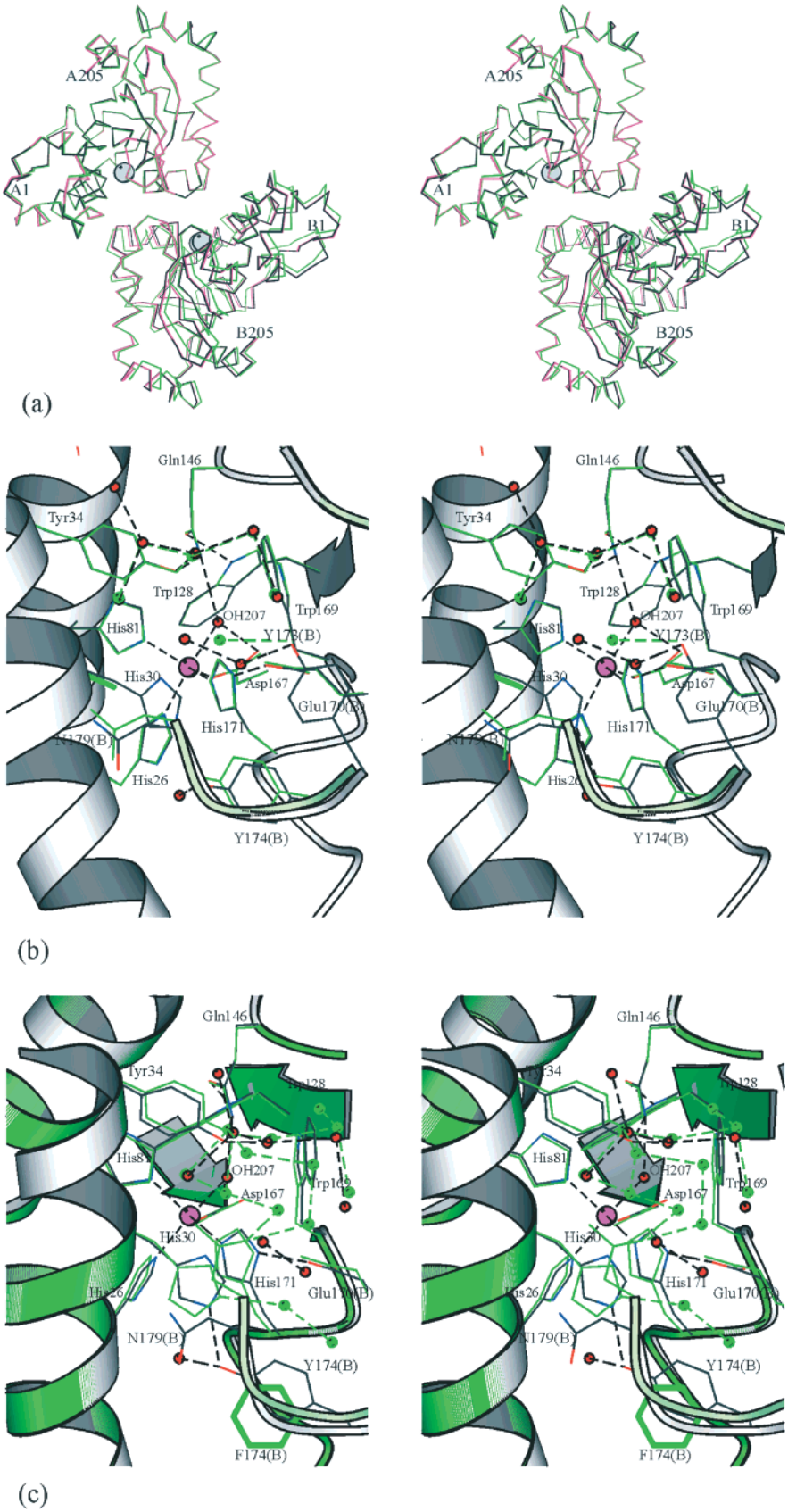

FIGURE 3: Structural comparison of wt MnSOD, H30A-MnSOD, and Y174F-MnSOD. (a) Superposition of dimers of wt MnSOD (black), H30A-MnSOD (dark pink), and Y174F-MnSOD (green). To show the relative orientations of subunits in the dimer, the superposition is for subunit A alone. The manganese ions are represented by gray spheres. (b) Superposition of H30A-MnSOD (green) onto wt MnSOD in the vicinity of the mutation site. (c) Superposition of Y174F-MnSOD (green) onto wt MnSOD in the vicinity of the mutation site. For the middle and bottom panels, the main-chain subunit B of the mutant is shown in light green. For the wt structures, side-chain oxygen atoms are colored red. The Mn ion is represented by a purple sphere. The figure was drawn with Molscript (*53*).

however, nonisomorphous with these structures, there being only a single dimer, rather than a pair of dimers, in the asymmetric unit, despite being crystallized at the same pH and under similar conditions to wt and H30A-MnSOD. At the pH of crystallization (8.0−8.3), His30 is unlikely to be charged. The dimers of Y174F-MnSOD are tightly packed in the unit cell, concomitant with a drop in solvent content from ∼55% for crystals of wt and other mutants to ∼46% for crystals of the Y174F mutant and with an increase in resolution from 2 to 2.3 Å to better than 1.35 Å. More numerous packing contacts around the A subunit of Y174F-MnSOD lead to an average *B* value somewhat lower than that for the B subunit and also to a larger scatter of side-chain torsion angles about their means for exposed and partly exposed residues compared to the scatter of that for wt and H30A-MnSOD. Careful analysis (*40*) of the differences in main-chain ϕ/ψ and side-chain χ_1/χ_2 torsion angles shows that these differences do not propagate beyond the affected residue, except in the vicinity of the mutated residue.

The structure of Y174F-MnSOD was determined at 110 K, whereas the structures of wt and other mutants (*37*) have been determined at ambient temperature. With few exceptions, solvent structure in the functionally interesting regions, such as the substrate-access funnel, the interdimer contact region, and cavities around the active site, is remarkably well conserved. Differences in these regions are generally an immediate consequence of the different polarity and steric requirements of the mutation. In particular, as discussed below, the altered orientation of subunits in the dimer of Y174F-MnSOD (Figure 3c) is not an artifact of crystal packing but is directly attributable to reorganization of hydrophobic packing of Leu175 and mutated residue Phe174 at the dimer interface.

Both mutants have more than 91% of residues in the most favored regions of the Ramachandran plot, as defined by PROCHECK (*54*) and as summarized in Table 2. As for wt and other mutants, for H30A and Y174F residue Gln178 falls into the generously allowed region (ϕ/ψ ∼50°/−120°). Similarly, residue Asn145 falls into the disallowed region (ϕ/ψ ∼45°/−115°) for H30A, but for Y174F, the value for ψ changes to −125°, placing this residue just inside the generously allowed region. Metal−ligand bond distances and angles of both H30A and Y174F mutants are very similar to those of wt MnSOD. In general, the Y174F structure shows less scatter of bond distances and angles and torsion angles about their mean values than is observed for H30A and wt MnSOD, notwithstanding the fact that, in contrast to strong NCS restraints applied to refinement of H30A and wt MnSOD, no NCS restraints were placed upon subunits of the dimer for refinement of the Y174F-MnSOD.

Structural Description of H30A. His30, whose side chain hydrogen bonds across the dimer interface to the side chain of Tyr174 of the other subunit, arises from the middle of helix A1. As a consequence, mutation of this residue to alanine has negligible effect on the main chain to which it is attached. Side-chain conformations of neighboring residues, such as metal ligand His26 and outer-sphere residue Tyr34, are also unaltered (see Figure 3b). However, across the dimer interface, the loop between β-strand B3 and helix A5 changes conformation slightly, leading to shifts of ∼0.5 Å in the position of Tyr174 OH and the side chain of the highly conserved Asn179 at the top of the substrate access funnel. With the exception of an additional solvent molecule between Ala30 CB and the phenyl ring of Tyr34, the space vacated by the mutation of the histidine to alanine is not occupied by water molecules, or at least by ordered water molecule(s). Rather, there is difference density to suggest that the side chain of Asn179, from the lip of the substrate access funnel, is disordered and partly occupies this site. This side chain rotates 160° in χ_1 to give an alternate position in which its terminal atoms occupy the approximate position vacated by His30 NE2. Nearer the surface and hydrogen-bonded to Y173(B) OH, a single water molecule in the H30A mutant replaces two in wt MnSOD. In addition to Asn179, disorder of nearby side chains of Tyr174, Gln178, Arg180, and Leu175 is apparent in the difference density, although alternative sites have low occupancy. Positions for partially occupied waters are also apparent. Overall, there is a loosening of the structure in the vicinity of the substrate access funnel.

Structural Description of Y174F. Tyr174 is largely buried in a hydrophobic pocket from which the OH moiety protrudes to hydrogen bond across the dimer interface with His30 NE2. On mutation to phenylalanine, the side chain retreats deeper into its hydrophobic pocket, expelling a water molecule that in wt MnSOD hydrogen bonds to the phenolic oxygen of Tyr174 and to the main-chain oxygen atom of metal ligand His171. In its new orientation, Phe174 makes hydrophobic contacts between 3.8 and 4.6 Å with Leu175 from the same subunit and with Ile25, Leu175, the CB of His171, and Phe174, all from the other subunit. This simple side-chain movement stimulates extensive rearrangements of neighboring residues in the dimer interface and large concerted shifts of the entire molecule, as the subunits within the dimer reorientate to accommodate the changes, as illustrated in Figure 3, panels a and c. The NCS axis relating the two subunits of the dimer is close to Tyr174. In the native structure the CD2 atoms of Tyr174 from each subunit of the dimer are 5.3 Å apart, whereas in the mutant structure the CD2 atoms of Phe174 are only 3.8 Å apart and, therefore, in hydrophobic contact. The CD2 atoms of Leu175 also move closer together from 4.3 Å in wt to within 3.7 Å in Y174F-MnSOD. Improved hydrophobic packing is the driving force for the reorganization and reorientation of the dimer interface and ultimately of the very different crystal packing of Y174F-MnSOD, compared to wt, H30A-, Y34F-, Q146H-, and Q146L-MnSOD (*18*, *37*).

The imidazole ring of His30, the partner in the hydrogen bond with Tyr174 of wt MnSOD, flips, changing χ_2 from −74 (2)° in wt to +75 (2)° in Y174F-MnSOD. The pattern of hydrogen bonding and also the uniformity of temperature factors around the ring are consistent with the assigned flipped orientation of His30. In its new position, the NE2 atom forms a 2.80 (3) Å hydrogen bond with an ordered water molecule in the substrate access funnel. This water molecule is not present in wt MnSOD. In addition, a nonclassical hydrogen bond of length 3.14 (5) Å exists between atom CD2 of His30 and another water molecule, which is tightly hydrogen-bonded [2.65 (4) Å] to the phenolic oxygen of outer-sphere residue Tyr34 and to two other water molecules [2.80 (4) and 2.73 (3) Å]. This ordered solvent is not present in subunits A and C of wt MnSOD but appears in subunits B and D, although shifted away from Tyr34 OH by ∼0.8 Å. In wt MnSOD the Tyr34 OH to His30 ND1

distance is 5.10 (6) Å. The equivalent distance to His30 CD2 in the Y174F mutant structure is 5.79 (7) Å, the distance increasing due to small rotations of these two residues away from each other, creating a larger space the better to accommodate a water molecule bridging H30 and Tyr34.

Changes in the dimer interface are propagated through to the active site, although the extent of change is small. Metal ligand His171 hydrogen bonds to the carboxylate moiety of Glu170 from the other subunit. Torsion angle χ_2 of Glu170 changes by 12° from a value of 177 (2)°, seen in all other *E. coli* MnSOD structures, to −173 (2)°. To maintain the hydrogen bond across the dimer interface, χ_2 of His171 changes from −124 (2)° to −116 (1)°. These changes are visible in Figure 3c.

As for the H30A-MnSOD, the side chain of the highly conserved Asn179 enjoys greater conformational freedom in Y174F-MnSOD than in wt MnSOD and Q146H-, Q146L-, and Y34F-MnSOD (*18*, *37*), where it is well ordered. For subunit B, Asn179 adopts a conformation similar to that observed in wt and to the major conformation of Asn179 in H30A-MnSOD, where the side chain points out toward the surface of the dimer. In subunit A of the Y174F mutant structure, the side chain is oriented into the substrate access funnel.

DISCUSSION

The hydrogen bond between the side chains of Tyr174 and His30 is an important element in the structures of Mn- and FeSODs. In sequence correlations, Tyr174 is absolutely conserved in Fe- and MnSODs and His30 is highly conserved, being replaced by asparagine in only 2 of 87 sequences examined (*40*), implying an essential role in the structure and function of all superoxide dismutases within this extended family. The side chains of these two residues arise from different subunits to form a hydrogen bond across the dimer interface. In hydrogen bonding to Tyr174 OH, His30 effectively buries Tyr174, and the exposed region of His30 forms part of the substrate access funnel. Mutation of His30 to alanine and substitution of Tyr174 by phenylalanine reduces the catalytic activity to 30% and 40% of wt MnSOD, respectively, a significantly greater reduction than that found for mutation of another gateway residue, Y34.

For H30A-MnSOD, this effect on activity is associated with a relatively localized and precise change in the structure: deletion of the imidazole ring. The H30A mutation does not appear to perturb the manganese coordination in the active site or disrupt other residues in the second coordination sphere (Figure 3b). Even Glu170(B), a second-sphere residue, which, like Tyr174, is provided by the *other* subunit, is not significantly affected by the mutation, and the water structure is minimally changed (Figure 3b). The major structural changes, other than the loss of His30, are the exposure of the Tyr174 phenolic oxygen and the occurrence of an alternate conformation for Asn179(B). In the H30A mutant, in place of the Tyr174 OH···NE2 His30 hydrogen bond, Tyr174 OH hydrogen bonds to a water (in subunit A) or to the side chain of Asn179(A) (in subunit B).

Structural changes due to the Y174F mutation are far more pervasive than those due to the H30A mutation, even though the same dimer interface hydrogen bond is broken in both cases. The driving force for the rearrangement of the dimer interface of Y174F appears to be the optimization of hydrophobic packing, as a result of the change in character of residue 174 from a polar tyrosine to a hydrophobic phenylalanine. The propensity of bulky hydrophobic residues to pack into solvent-excluded, nonpolar environments causes Phe174 of the Y174F mutant to undergo a greater conformational change than that which occurs for Tyr174 in the H30A mutant. The resulting movements of residues and main-chain atoms in the dimer interface propagate through the structure, resulting in small but possibly functionally significant changes in the active site, including reorientation of metal ligand His171, which affects the hydrogen-bonding arrangement of His171 with the Glu170 side chain across the dimer interface. The effect of the mutation on the position and orientation of His30 is particularly significant.

In the wt structure, the orientation of His30 is largely determined by the strong hydrogen bond between the NE2 nitrogen and Tyr174 that projects the ND1 nitrogen toward both the active site and Tyr34. In the Y174F mutant, the ring plane of His30 is effectively flipped, reversing the positions of its hydrogen-bonding groups. The decreased activity of the mutant enzyme suggests that the presence of the His30 ND1 amine N−H projecting into the substrate funnel may be important for optimizing the catalytic reaction. The most likely roles for the His30 ND1 nitrogen in turnover processes relate to its ability to form directed hydrogen bonds and to become deprotonated. Hydrogen bonding to the remote NE2 nitrogen is known to perturb the acidity of the histidine side chain; the interaction with Tyr174 may, therefore, not only orient His30 but also act to modify its effective pK_a. The ND1 N−H of His30 could thus be involved in orientation of the incoming substrate or protonation of the peroxide product. Movement of His30 also allows for solvent water to enter the space between His30 and Tyr34. This water is also present in the inactive iron-substituted MnSOD structure (*58*) but is not seen in the active wt enzyme (*18*).

Mn···OH Tyr34 and Tyr34 OH···NE2 His30 Separations as Determinants of Activity. In all native and wt Mn- and FeSODs, with the exception of the Tyr34-modified FeSOD from *Sulfolobus solfataricus* (*29*), the Mn···OH Tyr34 separation lies in the narrow range of 5.21 Å (*27*) to 5.48 Å (*19*−*21*). The MnSOD from *E. coli* has an Mn···OH Tyr34 separation of 5.38 (4) Å (*18*, *40*). In the H30A mutant this value is unchanged at 5.42 (7) Å, but in the Y174F mutant the separation increases to 5.76 (5) Å. In mutants of the outer-sphere residue Gln146, which hydrogen bonds to the OH^-/H_2O ligand, this separation decreases markedly as the Tyr34 side chain rotates into the solvent access funnel. For Q146L-MnSOD the separation is 4.92 (4) Å, and for Q146H-MnSOD it is 4.86 (2) Å (*37*). In human Q143N-MnSOD (*32*), the corresponding separation is also reduced to 5.04 (3) Å. In both wt and mutant Fe- and MnSODs, the Mn···ND1/CD2 His30 separations lie in the narrow range, 6.05 (5) Å (*18*, *40*) to 6.31 Å (*26*).

However, the separation His30 ND1···OH Tyr34 shows dramatic changes between wt and mutants; this separation effectively defines the size of the hole at the base of the substrate access funnel. For wt and native enzymes, this separation ranges from 4.73 (5) Å (*13*, *14*) to 5.16 (17) Å

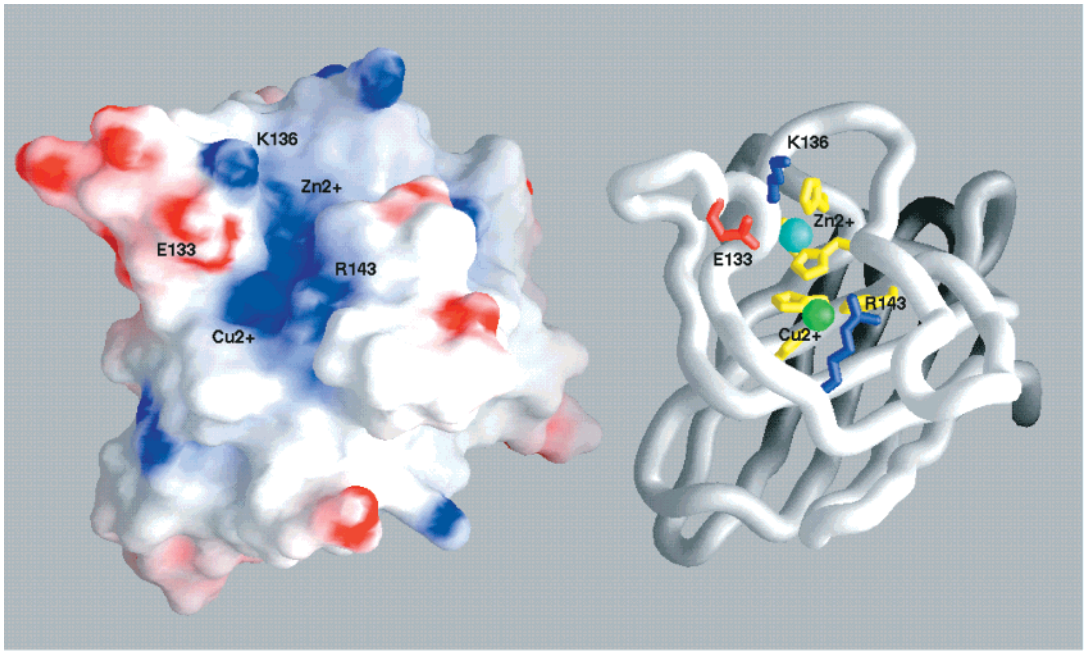

(a)

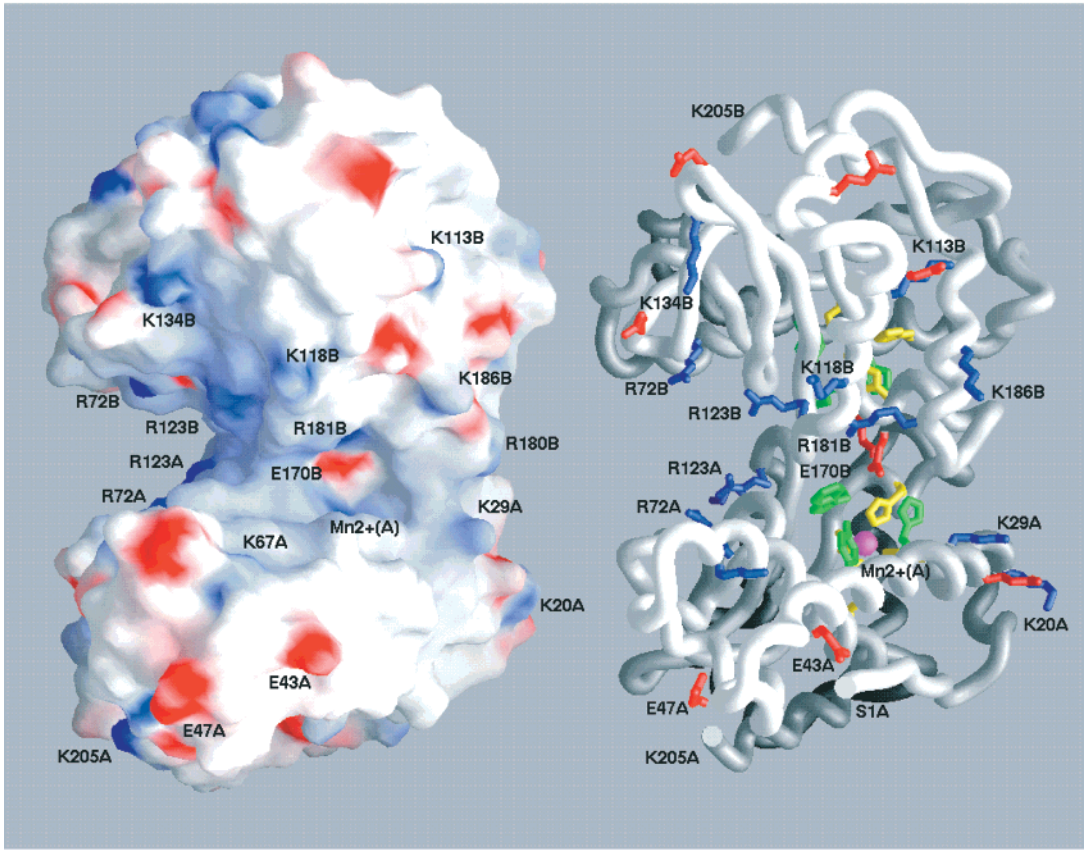

(b)

FIGURE 4: Comparison of substrate access regions of (a) CuZnSOD (yeast, PDB ID: 1JCV) and (b) MnSOD (*E. coli*, PDB ID: 1VEW). The left-hand panels show the surface defined by a probe atom of radius 1.4 Å and colored according to electrostatic potential (blue, positive; red, negative; extremes of color correspond to ~12*kT*). The right-hand panels show the polypeptide backbones and selected side chains (metal ligands, yellow; lysine and arginine, blue; aspartate and glutamate residues, red; gateway residues His30, Tyr34, and Trp169 of MnSOD, green). Metal ions are shown as spheres (green for Cu^{+}, aqua for Zn^{2+}, and purple for Mn^{2+}). The gateway residues (Trp169, Tyr34, and His30) and interface residue Glu170 are shown in green, and the Mn cation is shown as a purple sphere. Contrast the weakly positive electrostatic potential at the base of the substrate access funnel of MnSOD with that of CuZnSOD in the vicinity of the metal ions. Contrast also the greater complexity of the solvent access region of MnSOD compared to that of CuZnSOD. For MnSOD the suffixes A and B in the labeling denote the two subunits of the MnSOD dimer. Notice the long-range electrostatic potential created by the cluster of residues Arg72A and -B and Arg123A and -B on the left central side of the dimer. The figure was drawn with Grasp (*64*).

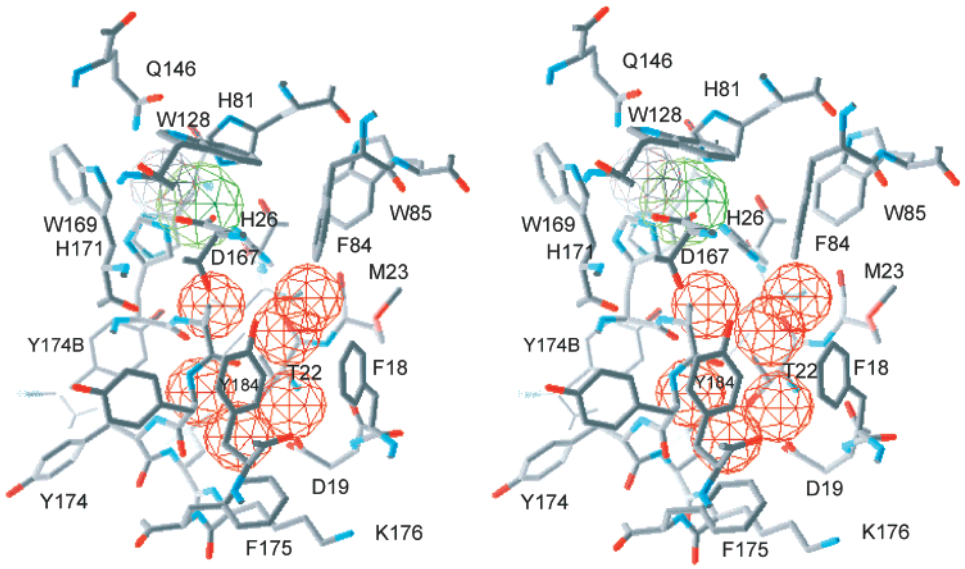

FIGURE 5: Stereo representation of the conserved internal water structure and channel that leads from metal ligand His26 to the surface, illustrated for wt MnSOD from *E. coli*. Water molecules, manganese, and the coordinated water/hydroxide species are shown, respectively, as wire mesh red, green, and gray balls of radius 1.4 Å. Protein atoms are conventionally colored by atom type. The figure was drawn with Grasp (*64*).

(*25*);[3] for MnSOD from *E. coli*, the separation is 5.09 (6) Å (*18*, *40*). For the H30A mutant of MnSOD from *E. coli* this distance does not exist, but for the Y174F mutant the distance increases to 5.79 (7) Å and because of the flip of the histidine ring involves atom CD2 not NE2 of His30. A water molecule occupies the expanded space. For Q146H and Q146L mutants (*37*), this separation is dramatically reduced to only 3.72 (2) and 4.23 (2) Å, squeezing out the water molecule found in subunits B and D between His30 and Tyr34 of wt MnSOD from *E. coli*. This water molecule is in general not conserved among Fe- and MnSODs. For the Q143N-MnSOD from *Homo sapiens* (*32*), His30 NE2···OH Tyr34 separation decreases by more than 0.5 Å relative to its value in wt MnSOD (*16*, *17*).[4] Thus, changes in this separation that lead to tightening of the substrate access funnel or to stabilization of water structure appear to lead to significantly diminished activity.

pH-Dependent Behavior. Wt MnSOD from *E. coli* and *H. sapiens* and wt FeSOD from *E. coli* all exhibit pH-dependent spectra, with an effective pK_a in the range 9.3−10.1 for titration of the visible absorption bands (*4*, *38*, *55*). This optical titration correlates with kinetic inhibition of dismutase activity in all cases where both properties have been measured. However, not all SOD derivatives exhibit this behavior. For example, the Y34A and Y34F mutants of *E. coli* MnSOD (*37*, *38*) and the H30A, H30N, and Y174F mutants described in the present paper all have pH-independent spectra in the range pH 5−10. The Y34F mutants of *E. coli* FeSOD (*56*) and human mitochondrial MnSOD (*31*) show similar pH-independent behavior. In the former enzyme, the pH-dependent spectral changes were attributed to deprotonation of Tyr34 (*56*) that is replaced by phenylalanine in the mutant, and, in the latter case, the transition is observed for the mutant but shifted to a much higher pK_a (11.1) (*31*). This pH-dependent spectral change has been attributed to binding of hydroxide at the sixth coordination site on the metal (*38*, *57*). Studies of Fe-substituted MnSOD indicate that the effect of the mutation is to shift this transition to higher pH values, suggesting that for the manganese-containing protein the effective pK_a lies beyond 10. This interpretation is supported by a crystal structure of Fe-substituted wt *E. coli* MnSOD, in which the sixth coordination site is clearly occupied (*58*).

A survey of well-characterized active site mutants for MnSOD suggests a simple classification can be made in terms of their pH dependence. For *E. coli* MnSOD, the solvent pocket mutants Q146H and Q146L both retain the pH sensitivity of the wt enzyme, whereas the substrate funnel mutants Y34F, Y34A, H30N, H30A, and Y174F are all insensitive to pH effects. Similarly, for human mitochondrial MnSOD, the solvent pocket mutant Q146N exhibits a pH-dependent transition (*32*), whereas the substrate funnel mutants H30Q, H30A, H30S, and Y34F are all effectively pH-independent below a pH of 11 (*34*). Thus, in general, mutations in the substrate funnel (but *not* the solvent pocket) affect the pH sensitivity, apparently decreasing the stability of the hydroxide adduct at high pH. The destabilization of the adduct may result from the loss of specific stabilizing hydrogen bonds (involving the funnel residues H30 and Y34) in the mutants.

Substrate Access to and Egress from the Active Site. Similar to the CuZnSOD family (*59*), the Mn- and FeSOD family (*11*, *12*, *60*, *61*) dismute superoxide at close to diffusion-limited rates. Although positively charged residues near the substrate funnel, together with the net +1 charge on the metal complex, may electrostatically guide superoxide ion into the active site (*62*, *63*), both families of SODs are

[3] For the cambialistic FeSOD from *Propionobacterium shermanii* [PDB ID: 1AR5 (*27*)], the short His31 CE1···OH Tyr168 hydrogen bond of 2.75 Å, the His31 CD2···O (H_2O) separation of 3.04 Å, and the absence of hydrogen bonds to His31 NE2 and His31 ND1 indicate that the histidine ring should be rotated 180° about χ_2 to give a more usual hydrogen-bonding arrangement. For the Q143N-MnSOD from *H. sapiens* [PDB ID: 1QNM (*32*)], a similar pattern indicates that one of the His30 rings should be flipped.

[4] In wt MnSOD from human mitochondria, abnormally short metal−ligand separations indicate that the metal-binding site was not fully occupied.

nonetheless extraordinarily efficient catalysts. They are structurally distinct, however, and profound differences exist between the substrate access channels of the CuZn family of SODs and the Fe and Mn family. For CuZnSODs, the active site lies in a shallow groove with several metal ligands substantially exposed, providing easy access for substrates to and departure of products from the Cu active site (Figure 4a). On the other hand, the active site in Fe- and MnSODs lies at the base of a 10 Å deep funnel, with the metal site and metal ligands almost completely buried, and only a weakly positive electrostatic potential at the molecular surface above the metal cation (Figure 4b), in contrast to the strongly positive electrostatic potential of the CuZnSOD. Ingress of superoxide and protons to, and egress of hydrogen peroxide and dioxygen from the active site are considered to occur through a narrow hole at the base of the substrate access funnel. This hole is defined by the side chains of Tyr34, His30, and Trp169 of one subunit and Glu170 from the other subunit. The orientation of subunits in this dimer is highly conserved in the structures of some 12 native, wt, and mutant Mn- and FeSODs, even for cases where the surface area buried in this interface is substantially less than the surface area buried by the dimer−dimer interface of the very strongly associated tetrameric SODs from, for example, *S. solfataricus* (*29*) and *Sulfolobus acidocaldarius* (*30*).

Thus, for Fe- and MnSODs, there appears to be a traffic problem with substrate and products each passing through the same small opening at rates in excess of 40 000 s^{-1}. Accordingly, we have examined closely the structures of most Fe- and MnSODs that have been reliably determined to date for potential alternative exits (or entrances) to the active site. Relative to the view down the substrate access funnel, there is a conserved, partially solvent-filled channel beginning behind ligand His26 that leads out to the protein surface in the vicinity of Asp19, at the turn between the extended N-terminal strand and the first helix. Figure 5 for wt MnSOD from *E. coli* shows these water molecules, which are highly conserved in the Fe- and MnSOD structures from 10 different organisms. While this channel is largely lined with hydrophobic residues, the main-chain peptide groups are exposed to offer hydrogen-bonding opportunities to the water molecules in this channel. This channel runs along the interface of the two domains that make up the monomer unit of Mn- and FeSODs. The first domain comprises the N-terminal extended chain and the two long α-helices (residues 1−86, which provide metal ligands His26 and His81); the second domain is an $\alpha\beta$ domain (residues 87−205). This hydrogen-bonding network also extends from His26 ND1 past Asp19 to OH Tyr174 from the other subunit (Figure 5). Immediately behind His26 is Phe84 (Tyr in some Fe- and MnSODs); a water molecule occupies approximately the position of the Tyr84 OH for those Mn- and FeSODs that have Phe at this position. Phe84 separates the aforementioned hydrogen-bonding network from a second network that runs between part of helix A2 (residues 83−86) and part of β-strand B (residues 163−165) to the surface of the protein and involves six water molecules. In all other structurally characterized Fe- and MnSODs a bulky group at Gly87 fills the bottom of this hole. While there is no obvious pathway from the vacant sixth coordination site—at which superoxide is believed to bind, at least in the M(III) half of the redox cycle—to either channel, breathing motions of the protein may open up transient gaps between the two domains to permit O_2 to enter the channel and diffuse to the surface. In the search for further clues as to how the family of Mn- and FeSODs achieve such high turnover despite severely restricted access to and exit from the active site via the substrate-access funnel, we suggest that residues in this putative channel are important targets for mutagenesis aimed at blocking the channel.

ACKNOWLEDGMENT

We gratefully acknowledge the assistance of Paul D. Hempstead, and of Victor Lamzin for facilitating access to the DESY synchrotron facility at Hamburg, Germany.

REFERENCES

1. McCord, J. M., and Fridovich, I. (1988) *Free Radical Biol. Med. 5*, 363−369.
2. Fridovich, I. (1995) *Annu. Rev. Biochem. 64*, 97−112.
3. Fridovich, I. (1997) *J. Biol. Chem. 272*, 18515−18517.
4. Bull, C., Niederhoffer, E. C., Yoshida, T., and Fee, J. A. (1991) *J. Am. Chem. Soc. 113*, 4069−4076.
5. Hsu, J. L., Hsieh, T., Tu, C., O'Connor, D., Nick, H. S., and Solverman, D. N. (1996) *J. Biol. Chem. 271*, 17687−17691.
6. McCord, J. M., and Fridovich, I. (1969) *J. Biol. Chem. 244*, 6049−6055.
7. Yost, F. J., Jr., and Fridovich, I. (1976) *J. Biol. Chem. 248*, 4905−4908.
8. Keele, B. B., Jr., McCord, J. M., and Fridovich, I. (1970) *J. Biol. Chem. 245*, 6176−6181.
9. Young, H.-D., Kim, E.-J., Roe, J.-H., Hah, Y. C., and Kang, S.-O. (1996) *Biochem. J. 318*, 889−896.
10. McCord, J. M. (1976) *Adv. Exp. Med. Biol. 74*, 540−550.
11. Parker, M. W., Blake, C. C. F., Barra, D., Bossa, F., Schinina, M. E., Bannister, W. H., and Bannister, J. V. (1987) *Protein Eng. 1*, 393−397.
12. Parker, M. W., and Blake, C. C. F. (1988) *FEBS Lett. 229*, 377−382.
13. Ludwig, M. L., Metzger, A. L., Pattridge, K. A., and Stallings, W. C. (1991) *J. Mol. Biol. 219*, 335−358.
14. Stallings, W. C., Pattridge, K. A., Strong, R. K., and Ludwig, M. L. (1985) *J. Biol. Chem. 260*, 16424−16432.
15. Parker, M. W., and Blake, C. C. F. (1988) *J. Mol. Biol. 199*, 649−661.
16. Wagner, U. G., Pattridge, K. A., Ludwig, M. L., Stallings, W. C., Werber, M. M., Oefner, F. F., and Sussman, J. L. (1993) *Protein Sci. 2*, 814−825.
17. Borgstahl, G. E. O., Parge, H. E., Hickey, M. J., Beyer, W. F., Jr., Hallewell, R. A., and Tainer, J. A. (1992) *Cell 71*, 107−118.
18. Edwards, R. A., Baker, H. M., Jameson, G. B., Whittaker, M. M., Whittaker, J. W., and Baker, E. N. (1998) *J. Biol. Inorg. Chem. 3*, 161−171.
19. Stallings, W. C., Powers, T. B., Pattridge, K. A., Fee, J. A., and Ludwig, M. L. (1983) *Proc. Natl. Acad. Sci. U.S.A. 80*, 3884−3888.
20. Carlioz, A., Ludwig, M. L., Stallings, W. C., Fee, J. A., Steinman, H. M., and Touati, D. (1988) *J. Biol. Chem. 263*, 1555−1562.
21. Lah, M. S., Dixon, M. M., Pattridge, K. A., Stallings, W. C., Fee, J. A., and Ludwig, M. L. (1995) *Biochemistry 34*, 1646−1660.
22. Ringe, D., Petsko, G. A., Yamakura, F., Suzuki, K., and Ohmori, D. (1983) *Proc. Natl. Acad. Sci. U.S.A. 80*, 3879−3883.
23. Stoddard, B. L., Howell, P. L., Ringe, D., and Petsko, G. A. (1990) *Biochemistry 29*, 8885−8893.
24. Stoddard, B. L., Ringe, D., and Petsko, G. A. (1990) *Protein Eng. 4*, 113−119.
25. Cooper, J. B., McIntyre, K., Badasso, M. O., Wood, S. P., Zhang, Y., Garbe, T. R., and Young, D. (1995) *J. Mol. Biol. 246*, 531−544.

26. Lim, J.-H., Yu, Y. G., Han, Y. S., Cho, S., Ahn, B.-Y., Kim, S.-H., and Cho, Y. (1997) *J. Mol. Biol. 270*, 259−274.
27. Schmidt, M., Meier, B., and Parak, F. (1996) *J. Biol. Inorg. Chem. 1*, 532−541.
28. Sugio, S., Hiraoka, B. Y., and Yamakura, F. (2000) *J. Biol. Chem. 267*, 3487−3495.
29. Ursby, T., Adinolfi, B. S., Al-Karadaghi, S., De Vendittis, E., and Bocchini, V. (1999) *J. Mol. Biol. 286*, 189−205.
30. Knapp, S., Kardinahl, S., Hellgren, N., Tibbelin, G., Schäfer, G., and Ladenstein, R. (1999) *J. Mol. Biol. 285*, 689−702.
31. Guan, Y., Hickey, M. J., Borgstahl, G. E. O., Hallewell, R. A., Lepock, J. R., O'Connor, D., Hsieh, Y., Nick, H. S., Silverman, D. N., and Tainer, J. A. (1998) *Biochemistry 37*, 4722−4730.
32. Hsieh, Y., Guan, Y., Tu, C., Bratt, P. J., Angerhofer, A., Lepock, J. R., Hickey, M. J., Tainer, J. A., Nick, H. S., and Silverman, D. N. (1998) *Biochemistry 37*, 4731−4739.
33. Cabelli, D. E., Guan, Y., Leveque, V., Hearn, A. S., Tainer, J. A., Nick, H. S., and Silverman, D. N. (1999) *Biochemistry 38*, 11686−11692.
34. Ramilo, C. A., Leveque, V., Guan, Y., Lepock, J. R., Tainer, J. A., Nick, H. S., and Silverman, D. N. (1999) *J. Biol. Chem. 274*, 27711−17716.
35. Leveque, V. J., Stroupe, M. E., Lepock, J. R., Cabelli, D. E., Tainer, J. A., Nick, H. S., and Silverman, D. N. (2000) *Biochemistry 39*, 7131−7137.
36. Bunting, K., Cooper, J. B., Badasso, M. O., Tickle, I. J., Newton, M., Wood, S. P., Zhang, Y., and Young, D. (1998) *Eur. J. Biochem. 251*, 795−803.
37. Edwards, R. A., Whittaker, M. M., Whittaker, J. W., Baker, E. N., and Jameson, G. B. (2001) *Biochemistry 40*, 15−27.
38. Whittaker, M. M., and Whittaker, J. W. (1997) *Biochemistry 36*, 8923−8931.
39. Whittaker, M. M., and Whittaker, J. W. (1998) *J. Biol. Chem. 273*, 22188−22193.
40. Edwards, R. A. (2000) Ph.D. Dissertation, Massey University, Palmerston North, New Zealand.
41. Hassett, D. J., Woodruff, W. A., Wozniak, D. J., Vasil, M. L., Cohen, M. S., and Ohman, D. E. (1993) *J. Bacteriol. 175*, 7658−7665.
42. Zhu, D., and Scandalios, J. G. (1993) *Proc. Natl. Acad. Sci. U.S.A. 90*, 9310−9314.
43. Touati, D. (1983) *J. Bacteriol. 155*, 1078−1087.
44. Carlioz, A., and Touati, D. (1986) *EMBO J. 5*, 623−630.
45. Whittaker, M. M., and Whittaker, J. W. (1991) *J. Am. Chem. Soc. 113*, 5528−5540.
46. Beyer, W. F., Jr., Reynolds, J. A., and Fridovich, I. (1989) *Biochemistry 28*, 4403−4409.
47. Otwinowski, Z., and Minor, W. (1997) *Methods Enzymol. 276*, 307−326.
48. Navazza, J. (1994) *Acta Crystallogr. A50*, 157−163.
49. Brunger, A. T., Adams, P., Clore, G. M., DeLano, W. L., Gros, P., Grosse-Kunstleve, R. W., Jiang, J.-S., Kuszewski, J., Nilges, M., Pannu, N. S., Read, R. J., Rice, L. M., Simonson, T., and Warren, G. L. (1998) *Acta Crystallogr. D54*, 905−921.
50. Cambillau, C., Roussel, A., Inisan, A.-G., and Knoops-Mouthuy, E. (1996) Bio-Graphics, AFMB-CNRS, Marseille, France.
51. Pannu, N. S., and Read, R. J. (1996) *Acta Crystallogr. A52*, 659−668.
52. Sheldrick, G. M., and Schneider, T. R. *Methods Enzymol. 277B*, 319−343.
53. Kraulis, P. J. (1991) *J. Appl. Crystallogr. 24*, 946−950.
54. Laskowski, R., MacArthur, M., Moss, D., and Thornton, J. (1993) *J. Appl. Crystallogr. 26*, 283−291.
55. Slykehouse, T. O., and Fee, J. A. (1976) *J. Biol. Chem. 251*, 5472−5477.
56. Sorkin, D. L., Duong, D. K., and Miller, A. F. (1997) *Biochemistry 36*, 8202−8208.
57. Yamakura, F., Kobayashi, K., Ue, H., and Konno, M. (1995) *Eur. J. Biochem. 227*, 700−706.
58. Edwards, R. A., Whittaker, M. M., Whittaker, J. W., Jameson, G. B., and Baker, E. N. (1998) *J. Am. Chem. Soc. 120*, 9684−9685.
59. Bertini, I., Mangani, S., and Viezzoli, M. S. (1998) *Adv. Inorg. Chem. 45*, 127−251.
60. Christianson, D. W. (1997) *Prog. Biophys. Mol. Biol. 67*, 217−251.
61. Whittaker, J. W. (1999) *Met. Ions Biol. Syst. 37*, 587−611.
62. Getzoff, E. D., Cabelli, D. E., Fisher, C. L., Parge, H. E., Viezzoli, M. S., banci, L., and Hallewell, R. A. (1992) *Nature 358*, 347−351.
63. Sines, J., Allison, S., Wierzbicki, A., and McCammon, J. A. (1990) *J. Phys. Chem. 94*, 959−961.
64. Nicholls, A., Sharp, K. A., and Honig, B. (1991) *Proteins: Struct., Funct., Genet. 11*, 281−296.

BI002403H